Application of Ru(II) Polypyridyl complexes in Metallopharmaceuticals and Material science

Sravani Gudikandula, Aruna Kodipaka, Navaneetha Nambigari *

Department of Chemistry, University College of Science, Saifabad, Osmania University, Hyderabad -500 004, Telangana State, INDIA.

Abstract: A series of three mononuclear ruthenium(II) polypyridyl complexes of the type $[Ru(A)_2qpd]$ $(ClO4)_2.2H_2O$, where qpd = N, N1-(8,9-Quinoxalinediylidene)-1,10-phenanthroline-5,6-diamine and A = (phen = 1,10 Phenanthroline (1), bpy = bipyridyl (2), tbz= 2-(1H-Pyrrol-2-yl)-1H-indole (3), were synthesized and characterized by several spectroscopic studies. The study focuses on DNA binding affinities, structural, nonlinear optical (NLO) properties, and docking interactions (with ds DNA) by both experimental (Biophysical methods – UV Absorption, Fluorescence, quenching, and viscosity) and computational (Density functional theory) methods.

The research shows that binding constant (K_b) values are in the order $1> 2 > 3$ for the Ru (II) polypyridyl complexes 1 to 3. The findings suggest that the phen and bpy complex has a stronger ability to bind with DNA than the tbz ligand, highlighting the importance of the auxiliary ligand. For molecular geometry (Ground State) and electronic characteristics using DFT calculations at B3LYP/LanL2DZ level. All complexes show an intense band due to metal to ligand CT band, n $\rightarrow\pi$* transition (HOMO to LUMO gap, Eg). The Eg gap of phen complex is most minor (2.0865 eV) compared to the Intercalator (2.5327eV). Among the three complexes, the phen complex has the most extended Intercalator length 15.8812 Å, and paramount optical properties. Further molecular docking predicted a DNA-binding preference for guanine, indicating a correlation with the experimental binding constant.

Keywords: Ru(II)polypyridyl complexes; DNA binding; DFT calculations; Nonlinear optical (NLO).

1. Introduction

Ruthenium complexes find applications directly or indirectly for a lot of problems related to anticancer drugs [1-5], materials science [3,4], polymers [6], and nanoscience [3,7-9] (Scheme 1). This is due to its versatile electron-transfer pathways [10-15]. Recent literature shows that ruthenium compounds are used in solar cells [16,17].
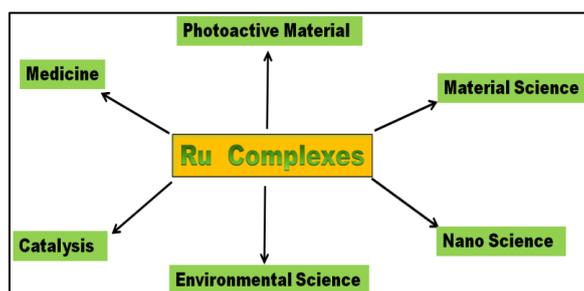
Scheme 1. Applications of Ru Complexes

Ru (II) can directly kill tumor cells due to excellent photophysical and chemical properties and different ligands. Combining their applicability as nanomaterials demonstrates enhanced antitumor efficacy. Several Ru(II) compounds exhibit improved antitumor activity owing to their water solubility [18,19]. Due to their unique photophysical, photochemical, and electrochemical characteristics, transition metal complexes containing polypyridine have received significant attention in recent years.

Studies about solar energy conversion, molecular electronics, light emitting devices, etc., the significance of metal complexes containing polypyridine ligands, such as 1,10-phenanthroline (phen) and 2,2 -bipyridyl (bpy), has been well documented [20]. According to the frontier molecular

orbital theory, the electronic characteristics of chemical compounds are primarily affected by the highest and lowest occupied molecular orbital (HOMO and LUMO). Due to its advantageous redox and optical properties, which can be easily modified by changing substitutions on the periphery and/or the element in the center of the bipyridine ring, bipyridine-fullerene systems are one of the most researched families of compounds among donor-acceptor systems [21].

Systems linked by van der Waals (vdW) forces, electrostatic interactions, stacking, metal-ligand coordination systems, and systems linked by hydrogen bonds have all been elegantly built and characterized [22-24]. In recent years, more focus has been placed on creating fullerene, porphyrin, and their derivatives to enhance solar cell performance. In their investigation of the development of photoactive fullerene/porphyrin complexes, Guldi et al. examined photo-induced charge transfer between C60 and coordination porphyrin pentamers (RuTPP.CO)4.(3-TPyP) and (RuTPP.CO)4.(4-TPyP) [25].

One of the most promising options for electrical and photonic applications in sustainable energy production, organic materials are the subject of constant and ardent research. The theory is that sunlight acts as the primary energetic source for a vast network of intricately linked biological processes necessary for the existence of life as we perceive it. Consequently, it is a desirable method to acquire clean energy to develop efficient and affordable devices that can capture, transform, and store solar; these technologies are only limited by human ingenuity [26,27]. To speed up forward electron transfer and lessen charge recombination, beautifully designed and evaluated enhanced model compounds with finely calibrated electronic coupling between the Donor–Acceptor (D-A) entities and well-adjusted D-A molecule energies have been established.

Owing to solid DNA binding ability and Optoelectronic properties, these complexes can be explored as DNA probes and nonlinear optoelectronic material, making them promising candidates for future biochemical studies and possible applications. In this paper, synthesis and characterization of three novel Ru(II) polypyridyl complexes. The ability of complexes to bind to DNA is measured using a combination of spectroscopic techniques, including UV-visible, fluorescence, and viscosity measurements. There have been molecular docking studies, and the results are consistent with the results of the experiments. The current research focuses on determining quantum chemical parameters using DFT to correlate the electronic structure with biological activity. Further development of new Ru (II) complexes of desired application and fine-tuning the property of Ru (II) complexes. Thus, this kind of study at the atomistic level of Polypyridyl complexes of Ru (II), moreover presents an insight of physicochemical, biochemical, spectrochemical, and materialistic details.

2. Experimental

2.1. Synthesis and Characterisation of Intercalator ligand and its Ru(II) Complexes

The precursor material was synthesized as per literature - 1,10-phenanthroline-5,6-dione (phendione) [28], cis-$[Ru(A)_2Cl_2] \cdot 2H_2O$, where A = phen, bpy and tbz [29]. A pictorial representation of the complexes of Ru(II) is given in Scheme 2.

Intercalator Ligand [N, N^1 –(8,9-Quinoxalinediylidene)-[1,10] phenanthroline-5,6-diamine)] was obtained by mixing phendione (0.525 gm, 2.5 mM) and Phenazine 2,3diamine (0.735 gm, 3.5 mM), Ammonium Acetate (3.88 gm, 50.0 mM), and 15ml of Glacial acetic acid for 4 hours, cool to room temperature and dilute with water. A yellow precipitate is collected by adding ammonia followed by washing with water, then recrystallized with $C_5H_5N.H_2O$ and dried in vacuo.

Anal. Data for $C_{24}H_{12}N_6$, Yield: 63.40%, Anal. Data: Calcd (%) C, H, N- 50.11, 2.78, 12.24; Found C, H, N - 52.02, 3.05,11.23; I R Data (KBr, cm^{-1}): 3377.36 (ν NH), 1118.71(ν CN).ES-MS (m/z) Calcd: 384.39; found: 385.56 [M+1].^{1}H-NMR (DMSO-d6, 400 MHz), δ (ppm):7.6-8(b,6H), 3.6(s, 4H), 2.92(t, 6H).

2.1.1. Synthesis of complexes (1-3) - Synthesis of [Ru (phen)$_2$ (qpd)](ClO$_4$)$_2$·2H$_2$O complex(1)

A light purple solution was formed over 8 hours of refluxing a mixture of qpd (0.192gm, 0.5 mM), Cis-$[Ru(phen)_2Cl_2]2H_2O$ (0.206 gm,0.5 mM), and ethanol (15 ml) at 120ºC, under N_2 atmosphere. Under vigorous stirring, an equal amount of saturated aqueous NaClO$_4$ solution was added. The mixture was cooled and filtered to eliminate the unreacted material. The red solid was dried under vacuum and followed by collection and washing with a tiny amount of water, ethanol, and diethyl ether.

Anal. Data for $C_{48}H_{28}N_{10}Ru$, Yield: 63.40%, Calcd (%) C, H, N - 51.21, 3.98, 11.95; Found C, H. N - 51.10, 4.05, 12.01;IR (KBr, cm^{-1}): 3408 (ν NH), 1083.99 (ν CN), and 621(ν Ru-N).ES-MS(m/z) Calcd: 845.87; found: 846.75 [M+1].^{1}H-NMR (DMSO-d6, 400 MHz), δ (ppm):7.5-8(b,6H), 3.4(s, 4H), 2.6(t,6H).
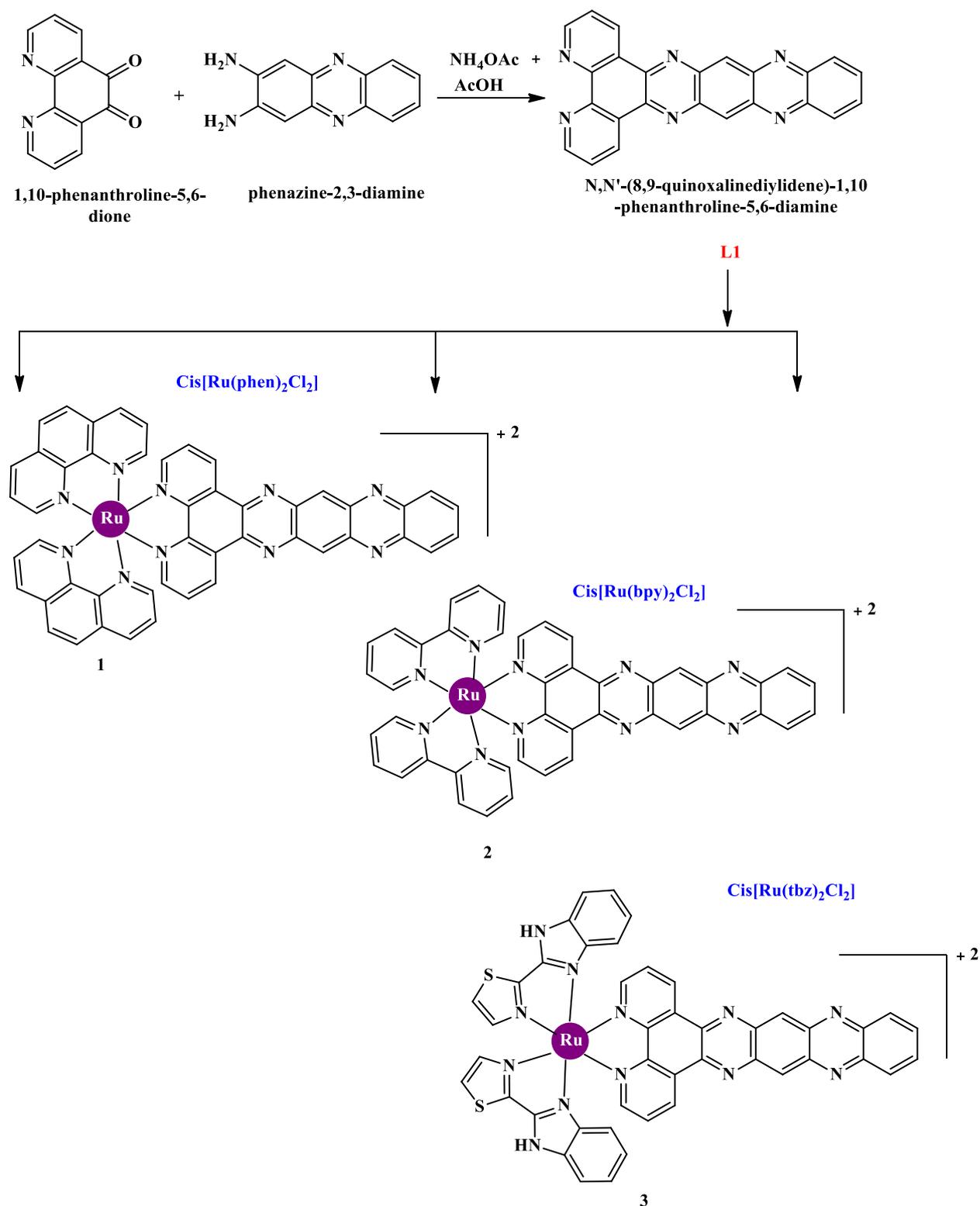
Scheme 2. Synthetic scheme for qpd (Intercalator) and Ru (II) Complexes

2.1.2. Synthesis of [Ru(bpy)₂(qpd)](ClO₄)₂·2H₂O complex(2)

Under an atmosphere of N_2, 8 hours were spent for refluxing a mixture of Cis- [Ru(bpy)$_2$Cl$_2$]2H$_2$O (0.26 g, 0.5mM), qpd (0.192g, 0.5mM), and ethanol (15ml)at 120ºC. After obtaining the pale purple solution, it cooled to room temperature, and an equal amount of saturated aqueous NaClO$_4$ solution was added. The brick-red material was collected and treated with ethanol, diethyl ether, and small amounts of water, then dried under a vacuum.

Anal. Data for $C_{44}H_{28}N_{10}Ru$ (Yield: 65.60%) Calcd (%) C, H, N - 52.34, 3.38, 11.30; Found: C, H, N - 51.98, 3.21, 11.25; IR (KBr, cm^{-1}): 3431(ν NH), 1083.99 (ν CN) and 621.08 (ν Ru-N).ES-MS(m/z) Calcd: 797.83; found: 797.93. ^{1}H-NMR (DMSO-d$_6$,

400 MHz), δ (ppm): δ 8.89 (b, 6H), 7.78(d, 6H), 7.63(s, 4H), 7.60(d, 2H), 3.4(s, 6H), 2.8(t, 4H).

2.1.3. Synthesis of [Ru (tbz)₂(qpd)](ClO₄)₂·2H₂O complex(3)

A mixture of qpd (0.192g ,0.5 mM), Cis-[Ru(tbz)₂Cl₂]2H₂0 (0.2g,0.5 mM), and ethanol (15 ml) was refluxed at 120ºC and under N₂ atmosphere for 8 hours, after vigorous stirring, an equal amount of saturated aqueous NaClO₄ solution was added. The mixture was cooled and filtered to eliminate the unreacted material. Solid was collected and washed with a tiny amount of water, ethanol, and diethyl ether. The red solid was then dried under a vacuum.

Anal. Data for $C_{44}H_{26}N_{12}RuS_2$ (Yield: 61.50%) Calcd (%) C, H, N -53.11, 4.36, 11.53; Found C, H, N -52.13, 4.21, 11.59; IR (KBr, cm⁻¹): 3421 (ν NH), 1087.85   (ν CN), and 621.08 (ν RuN). ES-MS(m/z) Calcd: 887.95; found: 888.94 [M+1].¹H-NMR (DMSO-d₆, 400MHz),δ(ppm):8.9(m,6H),7-8(m,6H), 5.9(t,2H), 2.9(t,2H), 3.5(s, 4H).

2.2. DNA Binding studies – Experimental and Computational

This section focuses on the methods used for the determination of DNA binding affinities, structural, nonlinear optical properties and docking interactions (with ds DNA) for three mononuclear Ruthenium (II) polypyridyl complexes by experimental studies as discussed in our protocols [30,31] (Details of Biophysical methods –UV Absorption, Fluorescence, quenching and viscosity studies are provided in Supplementary Data) and Computational methods (Density functional theory).

2.2.1. Computational details - Geometric optimizations

Ground state geometries and frontier molecular orbital (FMOs) of Ruthenium (II) complexes have been theoretically studied by the Density Functional Theory (DFT) method using two basis sets: LanL2DZ and a generic basis set in gas. DFT calculation is applied to understand the change in structural or geometrical parameters through calculations of bond length, bond angle, and torsional angle of metal complexes [32], besides the stability and reactivity of Ru(II) complexes are investigated [33].

Gaussian09 package was used to perform the DFT studies [34]. Initially, the molecules were subjected to optimization using the Semi-empirical PM₆ method in the gas phase [35]. The HOMO – LUMO transitions between the different orbitals were evaluated with DFT using the B3LYP [36,37] combined with the LanL2DZ [38] basis set for atoms C, H, N &Ru atom in a vacuum for equilibrium geometry at the ground state. The molecular geometry, the highest &lowest occupied molecular orbital (HOMO, LUMO) energies, and Mulliken atomic charges of the molecules are determined from optimized geometry (in Gas). Atomic charges of the ligand and Ru complex are calculated by the Mulliken method [39].The

Mulliken populace investigations, such as Atomic charges, electric dipole moment, polarizability, and first-order hyperpolarizability values were estimated.

The total energy, dipole moment, and energy of frontier orbital (HOMO-LUMO) were all calculated using DFT studies. The molecular properties, such as the chemical potentials (P_i), HOMO-LUMO gap (E_g), absolute hardness(η), absolute electronegativity (χ), absolute softness (σ), global electrophilicity (ω), global softness (S), and electronic charge, N_{max} were calculated according to the equations 1 – 8 [40,41].

$$Eg = ELUMO - EHOMO$$
(1)

$$\chi = \frac{EHOMO + ELUMO)}{2}$$
(2)

$$\eta = \frac{(ELUMO - EHOMO)}{2}$$
(3)

$$\sigma = \frac{1}{\eta}$$
(4)

$$Pi = -\chi$$
(5)

$$S = \frac{1}{2\eta}$$
(6)

$$\omega = \frac{Pi^2}{2\eta}$$
(7)

$$\Delta NMax = \frac{-Pi}{\eta}$$
(8)

From the HOMO - LUMO energy gap (Eg) reactivity of the complex can be accessed; the narrow gap suggests high complex reactivity [40,42]. The Optoelectronic behavior is extensively studied due to its immense uses in developing communications technologies, optical interconnections, and signal processing [43].

The finite perturbation method was applied for the calculation of polarizability (α_o) and hyperpolarizability (β_o) [44]. The magnitude of the mean first hyperpolarizability tensor was calculated by using x, y, and z components from Gaussian output. The wide-ranging equations (Eq. 9 – 11) were used to calculate the dipole moment (μ_{tot}), the polarizability (α_o), and the first order hyper polarizability (β_o) [45] from the x, y, and z components.

$$\mu_{tot} = (\mu_x^2 + \mu_y^2 + \mu_z^2)^{1/2}$$
(9)

$$\alpha_o = 1/3 \, (\alpha_{xx} + \alpha_{yy} + \alpha_{zz})$$
(10)

$$\beta_o = [(\beta_{xxx} + \beta_{xyy} + \beta_{xzz})^2 + (\beta_{yyy} + \beta_{yzz} + \beta_{yxx})^2 + (\beta_{zzz} + \beta_{zxx} + \beta_{zyy})^2]^{1/2}$$
(11)

The value of the polarizabilities (α) and the hyper polarizabilities are given in atomic units (au.), and are converted to electronic units (e.s.u.) (for α: 1au. = 0.1482×10^{-24}esu and for β: 1 au = $0.0086393 \times 10^{-30}$ esu).

The DNA sequence (Receptor) *[5'-D (AP CP GP AP CP GP TP CP GP GP GT) 3']*of PDB id: **423D** (https://www.rcsb.org/) and the 3D conformer of Ru (II) complex (Ligand) are the inputs utilized for docking using the Patch Dock tool [46]. Polar hydrogen was added to the receptor after the heteroatoms and water were removed before uploading the DNA PDB file and the metal complexes' 3D conformers with the program parameter set to its default values. The Docking server works on the criterion of shape complementarity and scoring functions. The results are a set of docked poses, which were further evaluated on the basis of Atomic Contact energy (ACE).

3. Results and Discussion

This section discusses the analysis of spectral characterization and the structural, biological chemical descriptors, and nonlinear optical properties (Density functional theory study). Also, the Biophysical methods – UV Absorption, Fluorescence, viscosity, and docking interactions (with ds DNA) for three mononuclear ruthenium (II) polypyridyl complexes.

3.1. Spectral characterization of complexes

Spectroscopic techniques such as FT-IR, UV, ^{1}H NMR, and elemental analysis were used for structural evaluation of the Intercalator ligand and Ru complexes (1-3). The complex formation is also evident in the FTIR spectra of the three complexes. Comparing the FTIR spectra of the ligand and complexes revealed frequency changes. In the IR spectra of the ligand (qpd), vibrations at ν (NH) at 3377 cm^{-1} and ν(CN) at 1029 cm^{-1} are shifted to ~3541 cm^{-1} and ~1083 cm^{-1} after the Ru complex is formed, and also Ru–N band appeared at 621 cm^{-1} [47]. (IR spectra of complexes (Figure S1 – S4) are given in Supplementary Data).

The absorption spectra of the three complexes showed MLCT bands at 462 nm, 457 nm, and 467 nm, respectively, which were not present in the qpd ligand, indicating the complex formation [48]. ^{1}H NMR spectra of the complexes showed peaks downfield as compared to the ligand (qpd), indicating complexation. The signals for phen appear at 7.6 to 8.5 ppm, for tbz in the range of 7.0 to 8.0 ppm, bpy in the range of 7.5 to 8.9, the ligand qpd hydrogen's appeared at 6.0 to 8ppm (Aromatic) and ~2.6 and 3.4ppm. (^{1}H NMR spectra of complexes (Figure S5 – S7) are given in supplementary Data).

3.2. Biophysical Studies - UV-Visible absorption, Fluorescence, quenching, and viscosity studies

The interaction of metal complexes with DNA can be studied using electronic absorption spectroscopy. The redshift (hypochromic shift) in the MLCT (metal to ligand charge transfer) band is connected to the Metallo Intercalator—DNA binding. It is caused by intercalation, including potent stacking interactions between DNA base pairs and an aromatic chromophore. The intensity of the interaction is inversely correlated with the magnitude of the hypochromic shift. Therefore, spectroscopic titrations with varying concentrations of CT-DNA were investigated to offer proof for the probability of binding for each complex. Figure 1 displays the complex's distinctive spectral profile at various DNA concentrations. The MLCT bands of complexes at 462 nm (1), 457nm (2), and 467nm (3) [49], exhibit a hypochromic shift of around 12.01,14.01, 13.0%, respectively, and bathochromic shift of approximately 10-30 nm as the DNA concentration increased.

The intrinsic binding constant K_b measured in each case by analyzing the variations in their absorbance with increasing concentration of CT-DNA at MLCT band helped further to clarify the power of the complex binding to DNA. The K_b values for complexes 1 - 3 are $8.0 \times 10^4, 2.5 \times 10^4, 1.5 \times 10^4$, respectively. The K_b values are higher than the parent complex [Ru(phen)$_3$]$^{+2}$($K_b = 5.5 \times 10^3$ M^{-1}), but lower than DNA metallo intercalators like [Ru(dppz)(bpy)$_2$]$^{+2}$, which has a $K_b > 10^6$ M^{-1} [50]. From the above data, the order of binding strength of Ruthenium complexes with CT-DNA is 1 > 2 > 3. This may be due to the more planarity of phen ancillary ligand in complex 1.

The dppz ligand possesses a large aromatic surface area, intercalator length, and more, allowing extensive intercalation in the DNA base pairs and an accompanying increase in metal-to-ligand charge transfer (MLCT). Based on most Ru polypyridine complexes, the ligand binds strongly to the DNA duplex via the intercalation mechanism. The Barton group initially discovered the ability of [Ru(bpy)2dppz]$^{2+}$ to function as a non-radioactive luminous DNA probe. At room temperature, this combination exhibits no photoluminescence, but when double-helix DNA is present, it exhibits intense photoluminescence with an enhancement factor of >10^4. The DNA "light-switch" effect, which is a phenomenon that has received a lot of interest, has been extensively used to explore how metal polypyridyl complexes interact with DNA [51].
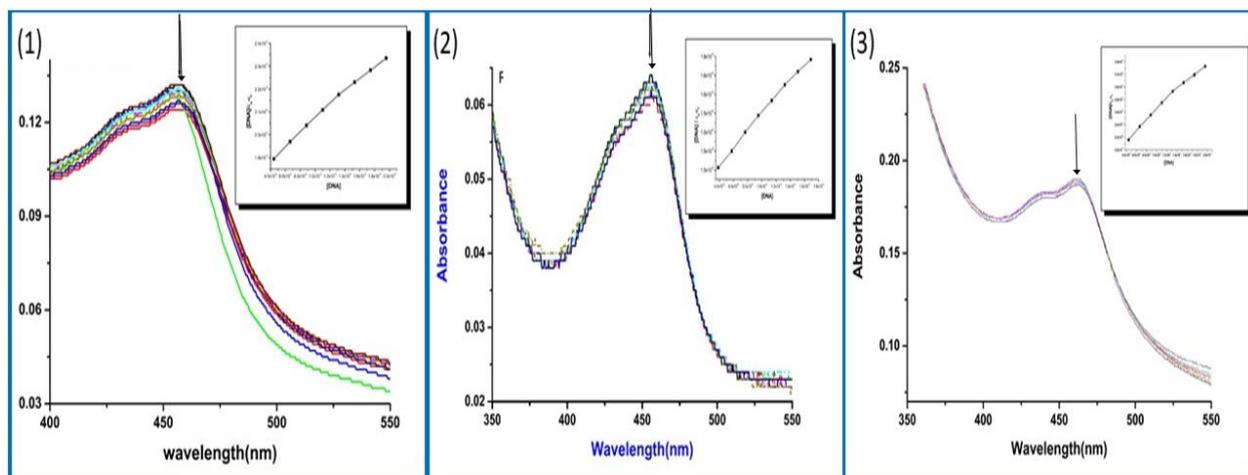
Figure 1. Absorption spectra of complexes (1 to 3) in the presence (lower) and absence (top) of DNA in Tris–HCl buffer. The 10 μL of stock complex concentration (0.001 M) is added in the cuvette, and DNA $(0.617 \times 10^{-4}$ M) is added in the range of 0–120 μL. Changes upon increase of DNA concentration is represented with the arrows, inserted a plot by taking [DNA]/(εa–εf) vs [DNA] gives intrinsic binding constant (K_b). 1) $[Ru(phen)_2qpd]^{+2}$, 2).$[Ru(bpy)_2qpd]^{+2}$,3). $[Ru(tbz)_2qpd]^{+2}$

Luminescence investigations performed at a constant metal complex concentration (5 mM) in Tris buffer (pH 7.2) at room temperature can explain the precise nature of binding for metal complex - DNA. The degree to which the complex integrates into the DNA's hydrophobic environment is correlated with the change in emission intensity. In the presence of various concentrations of CT-DNA, Figure 2 displays the fluorescence emission spectra for the free and bound complexes 1 to 3. The excitation wavelength for the three complexes considered at 452, 465, and 470, respectively, and the emission wavelengths of complexes 1 to 3 are observed at 602, 604, and 614 nm. With the increase in DNA concentration in the complex (1–3), the fluorescence intensity increases.
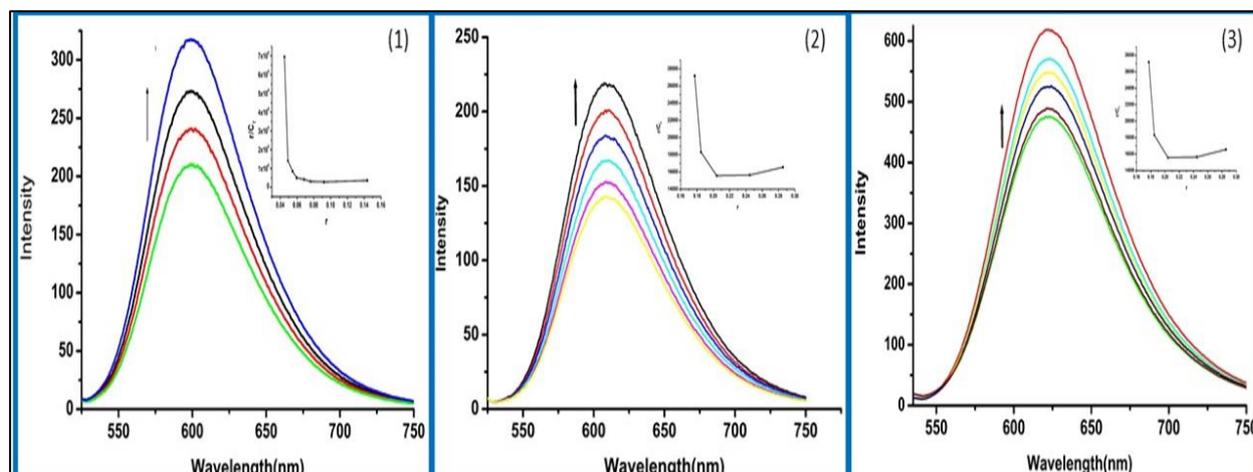
Figure 2. Emission spectra of Ruthenium (II) complexes by addition of CT-DNAin Tris–HCl buffer. The arrow shows the intensity variation by incremental addition of DNA. Inset: Scatchard plot of the complexes, from which binding constant (K_b) calculated.1) $[Ru(phen)_2qpd]^{+2}$, 2). $[Ru(bpy)_2qpd]^{+2}$, 3). $[Ru(tbz)_2qpd]^{+2}$

The plot of r/C_f vs r on the basis of a modified Scatchard equation, where r is the binding ratio C_b/[DNA] and C_f is the concentration of free ligand, determines the intrinsic binding constant from the luminescence data. The binding constants (K_b) for complexes 1 to 3 were 8.2×10^4 M^{-1}, 4.9×10^4 M^{-1}and 3.5×10^4 M^{-1}, respectively, according to Scatchard plots for the complexes built from luminescence spectra.
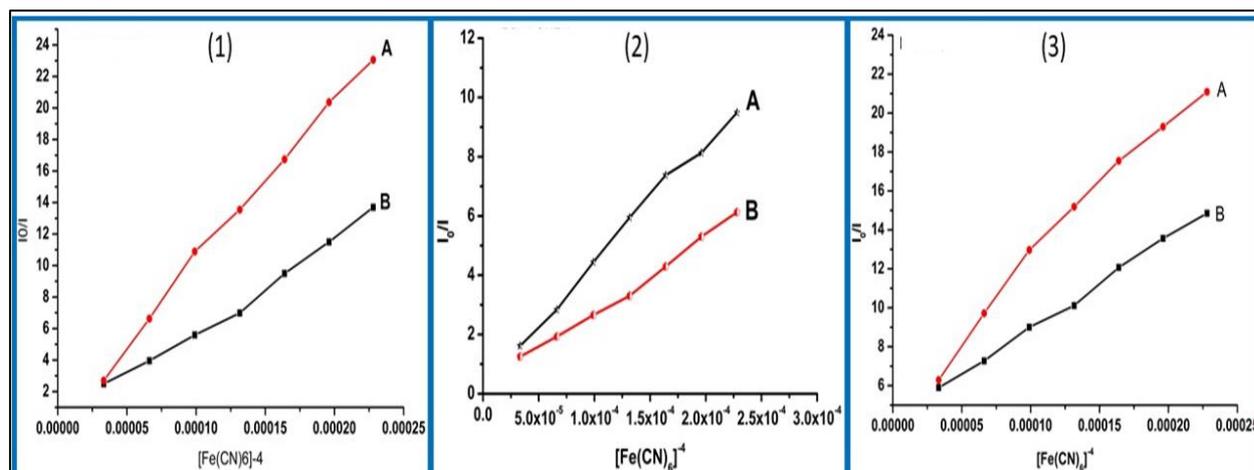
Figure 3. Quenching studies of the complex with $[Fe(CN)_6]^{-4}$ in Tris-HCl in the absence (A) & and presence of DNA (B).1) $[Ru(phen)_2qpd]^{+2}$, 2). $[Ru(bpy)_2qpd]^{+2}$, 3). $[Ru(tbz)_2qpd]^{+2}$

Compared to the intensity in the absence of CT-DNA, the fluorescence intensities of complexes were increased by 6.27, 5.52, and 4.83 times respectively [52]. The complex emission was modest due to the lack of DNA, but adding DNA causes the emission intensity to increase until capacity is attained (concentrated emission strength), which is caused by the complex being attached to DNA. The mobility of the complex is constrained at the binding site due to the intercalation into the DNA base pairs. The DNA helix's hydrophobic environment restricts the complex's access to solvent molecules, which lowers the stretching vibrations of relaxation.

Fluorescence quenching studies performed in the presence of $[Fe(CN)_6]^{-4}$ as a quencher provide additional information about the binding of complexes to complexes to DNA. In the presence or absence of DNA, all three complexes were quenched with increasing amounts of $[Fe(CN)_6]^{-4}$ as shown in Figure 3, and the data were then analyzed using the Stern-Volmer equation.

Table 1. Intrinsic Binding constant of Ru (II) complexes with CT-DNA.

Complex	$K_b (M^{-1})$ (Absorption)	$K_b (M^{-1})$ (Emission)	K_{sv} value Without DNA	K_{sv} value With DNA
$[Ru(phen)_2(qpd)]^{+2}$	8.0×10^4	8.2×10^4	20,280	354.24
$[Ru(bpy)_2(qpd)]^{+2}$	2.5×10^4	4.9×10^4	11,345	298.02
$[Ru(tbz)_2(qpd)]^{+2}$	1.5×10^4	3.5×10^4	10,051	210.57

The complexes effectively quench due to quencher in the absence of DNA. Still, there was little quenching in the presence of DNA because the powerfully negatively charged $[Fe(CN_6)]^{-4}$ would be repelled by the negatively charged DNA phosphate backbone [53,54], which would prevent the quenching of the bound complexes. Table 1 also includes the K_{sv} values in addition to the K_b values. Complexes' DNA binding affinities are consistent with the following findings, according to quenching studies.

The lack of crystallographic data, indicative of the DNA viscosity measurements to be considered as the least obscure and crucial assessment of a DNA binding model and giving a compelling indication of the intercalative binding mode is viscosity [55]. A traditional intercalation model, in which base pairs are removed to free up space for the binding ligand, lengthens the DNA helix and raises DNA viscosity. However, some non-classical intercalation of the ligand may cause the DNA helix to bend or curl, shortening its effective length. For instance, in the right circumstances, the intercalation of a dye like ethidium bromide (EtBr) roots an increase in the length of the DNA as a whole.
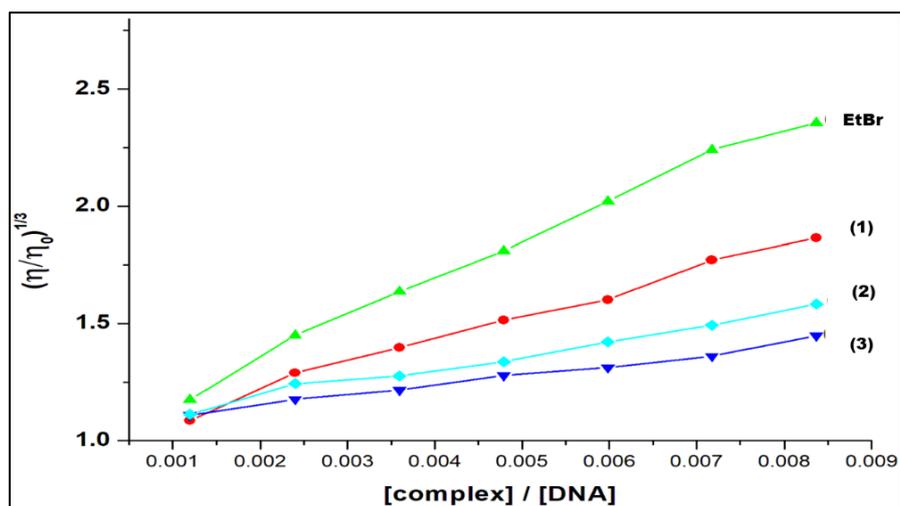
Figure 4. Viscosity Study of calf thymus DNA at room temperature in BPE buffer with increase in the concentration of complex. [(1) [Ru(phen)$_2$(qpd)]$^{+2}$, (2) [Ru(bpy)$_2$(qpd)]$^{+2}$, (3) [Ru(tbz)$_2$(qpd)]$^{+2}$and ethidium bromide (EtBr)

Figure 4 shows the difference in the viscosity between DNA and EtBr because of the metal complexes. Although the intercalating ligand is the same in each molecule, the variations in the ancillary ligands are what affect viscosity.

In accordance with the results of the absorbance titration, the results further reveal that three Ru(II) complexes exhibit an intercalative binding mechanism to CT-DNA. The complexes continue to adhere to DNA like earlier techniques have demonstrated. Viscosity order of the complexes follows EtBr > [Ru(phen)$_2$(qpd)]$^{+2}$> [Ru(bpy)$_2$(qpd)]$^{+2}$> [Ru(tbz)$_2$(qpd)]$^{+2}$.This is because of the difference in the auxiliary ligands attached to the Ruthenium (II) metal ion.

3.3. Computational Studies - DFT
The analytical and spectral studies depict the octahedral coordination of Ru(II) complexes, further verified by their molecular modeling studies. The 3D-optimized Ru complexes are presented in Figure S8. The energy minimization was iteratively repeated to find out the total energy, which is as follows: -2486.7551(phen), -2319.2161 (bpy), 2462.7542 (tbz) a.u. respectively, indicating a more stable phen complex. Further, conformational analysis of Ru (II)

polypyridyl complexes viz bond length, bond angles, torsion angles, and Intercalator lengths reveal vast structural information like the bond strength, distortions, etc.

The structural data (Ru - N bond length and Ru - Intercalator length) of the Ru complex conformers are shown in Table 2. Ru – N bond length (N of ancillary ligand) in 2.1 ± 0.01 Å complex, whereas Ru – N (N of Intercalator-qpd) is shorter. The Intercalator length is short for the bpy and tbz complex indicating an ineffective intercalation, whereas the phen complex is expected to show an effective binding with DNA. The bond angles in all the complexes were reasonably close to an octahedral geometry of ~89.1 - 96.1°, but strain-revealing optimized architectures are distorted octahedrons. Additionally, the dihedral angles show eccentricity in all the complexes. The dihedral angle assessment reveals that complexes 2 and 3 are more disordered from planarity. This led to the conclusion that complexes have conformational differences. The bond length values obtained from the 3D optimization were in the range 2.1 ± 0.01 Å for the Ru(II) polypyridyl complexes with phen, bpy and tbz ancillary ligands, which were similar to the previously reported complexes [56,57].

Table 2. Bond and Intercalator lengths of the 3D conformers of Ru - qpd complexes.

Complex	Intercalator length (Å)	Bond lengths(Å)					
		M- N$_1^a$	M- N$_2^a$	M- N$_3^b$	M- N$_4^b$	M- N$_5^b$	M- N$_6^b$
[Ru(phen)$_2$qpd]$^{+2}$	15.8812	2.10679	2.10546	2.10679	2.10543	2.10598	2.10594
[Ru(bpy)$_2$qpd]$^{+2}$	15.8206	2.17735	2.17733	2.17646	2.17653	2.18157	2.18162
[Ru(tbz)$_2$qpd]$^{+2}$	15.8691	2.11265	2.11444	2.12226	2.10794	2.09697	2.09322

The bond lengths (b: N3, N4, N5, N6, are nitrogen polypyridyl (phen, bpy, tbz) bonded to Ru. a: N1 and N2, N of qpd ligand bonded to Ru).

The frontier molecular energy levels [HOMO (Highest Occupied Molecular Orbital) and LUMO (Lowest Unoccupied Molecular Orbital)] for Metal Polypyridyl complexes furnish insight into the potential electronic transitions. The Energy difference between HOMO and LUMO orbital is called an energy gap and is also believed to be an important parameter to determine the stability of the structure.

Table 3. Data for HOMO, LUMO, IP, EA, and LUMO- HOMO gap (Eg).

Parameter (eV)	qpd	Complex 1	Complex 2	Complex 3
HOMO	-6.2119	-9.5357	-9.5403	-9.5324
LUMO	-3.6791	-7.4492	-6.9678	-7.5757
Eg, (LUMO-HOMO gap)	2.5327	2.0865	2.5724	1.9567
Ionization potential (I)	6.2119	9.5357	9.5403	9.5324
Electron affinity (A)	3.6791	7.4492	6.9678	7.5757

The HOMO and LUMO, LUMO-HOMO energy gap indicate the electrophilic-nucleophilic nature of the molecule and also the utmost vital measure of chemical reactivity. The data of the LUMO - HOMO gap (Eg), ionization potential, and electron affinity of ligand, qpd, and its complexes are given in Table 3.

The energy gaps in complex 1 - 3 are found to be in the range of 1.9567 eV to 2.5724 eV, whereas qpd Ligand (2.5327 eV) shows less chemical activity than the corresponding Ru(II) complexes. Among the complexes, the tbz complex is more reactive than the phen and bpy complexes. Figure 5 shows the 3D Contour surfaces of the frontier molecular orbitals of the Ligand, qpd, and Complexes.

LUMO	-3.6791	-7.4492	-9.6678	-7.5757
Eg	2.5327	2.0865	2.5724	1.9567
HOMO	-6.2119	-9.5357	-9.5403	-9.5324
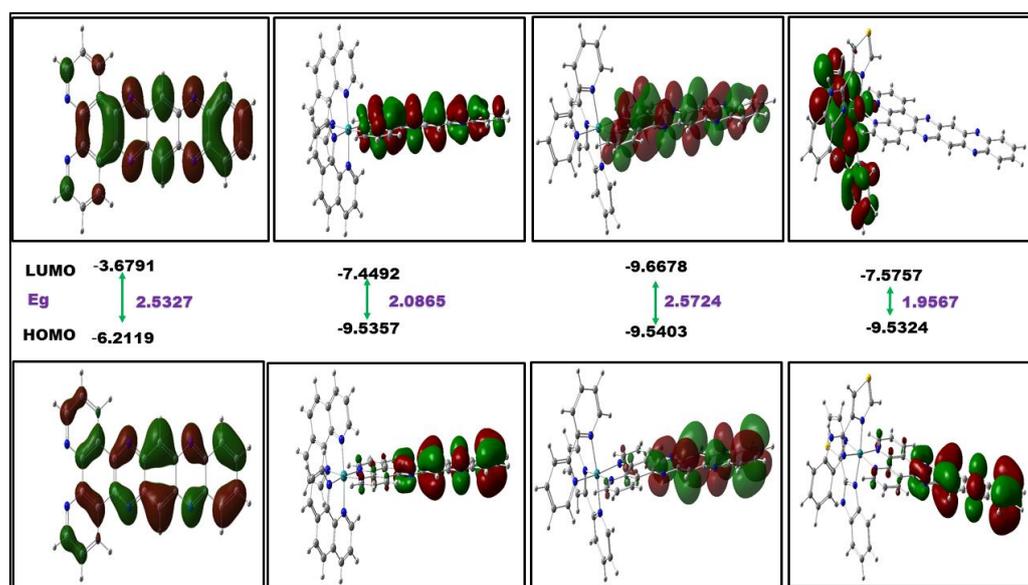
Figure 5. HOMO - LUMO energy gap of the complexes·1) [Ru(phen)$_2$qpd]$^{+2}$, 2). [Ru(bpy)$_2$qpd]$^{+2}$, 3). [Ru(tbz)$_2$qpd]$^{+2}$

The HOMO–LUMO energy display shows that complexes 1 & 3 are more susceptible to nucleophilic attack than complexes 2. The 3D contour diagrams show that the LUMO of the complex is centralized principally on or around Ru (II) cation and ancillary ligands (tbz). In contrast, the HOMO is restricted to the Quinoxaline ring of the Intercalator, qpd. The frontier orbitals of complexes 1 and 2 are similar and confined chiefly on the Quinoxaline ring. The results display that the LUMO of transition metal ions tends to lower the HOMO orbital of nitrogen atoms of the Quinoxaline ring of the Ligand.

The molecular parameters are calculated to predict the biological and chemical reactivity. Absolute hardness (η), a derivative of total energy and electronegativity was used to establish the principle of hard and soft acids and bases. Global Electrophilicity (ω) is the measure of the extent of the electrophilicity of a molecule. The chemical potential (μ) reflects the global reactivity index, translated as a charge transition from a higher chemical potential system to a lower chemical potential system. Electronegativity (χ) represents the ability to draw electrons equal to the negative of the chemical potential.

Table 4 lists the characteristics of Biological and Chemical reactivity parameters that were computed as a product utilizing the energies of the frontier molecular orbitals (LUMO, HOMO). According to Parr et al. [58], the amount of a molecule's electrophilicity is measured by the "electrophilicity index," which is an encouraging and sure measure of overall reactivity, chemical hardness, and potential. This novel reactivity index has been developed to track energy stabilization when the system picks up an extra electronic charge (N) from the surrounding environment.

Table 4. Biological and Chemical reactivity parameters.

Parameters	qpd	Complex 1	Complex 2	Complex 3
Absolute Hardness, (η)	1.2663	1.0432	1.2862	0.9783
Absolute Softness, (σ)	0.7896	0.9585	0.7774	1.0221
Global Electrophilicity (ω),	9.6567	34.5656	26.4839	37.3954
Chemical potential, (μ)	-4.9455	-8.4924	-8.2540	-8.5540
Absolute Electronegativity, (χ)	4.9455	8.4924	7.6962	8.5540
Global softness, S	0.6331	0.5216	0.6431	0.4891
Additional Electronic charge, ΔN_{max}	3.9052	8.1403	6.4171	8.7432

Most commonly, molecular orbital energy is used to assess reactions and their active sites in conjugated systems [59]. The HOMO, LUMO, and energy gap play a significant role in determining their natural function. The ionization potential and HOMO's energy are intimately related due to its electron donation tendency. Although the LUMO can pick up electrons, electron affinity is highly correlated with LUMO energy [60,61]. A molecule with a small frontier orbital gap with elevated chemical reactivity and low kinetic stability is typically more susceptible to polarization [62].

Mulliken charges are the outcome of the Mulliken population analysis and offer a way to calculate partial atomic charges using computational chemistry methods, notably those that rely on the linear combination of atomic orbitals molecular orbital approach. One of the crucial elements directly related to the vibrational properties of the molecule is the Mulliken atomic charge. To comprehend the electrical structure, this component affects several molecular characteristics, including polarizability, dipole moment, and electronic structure [63,64]. The atomic charges obtained by Mulliken analysis of Ru complexes are shown in Table S1 and in Figure 6.
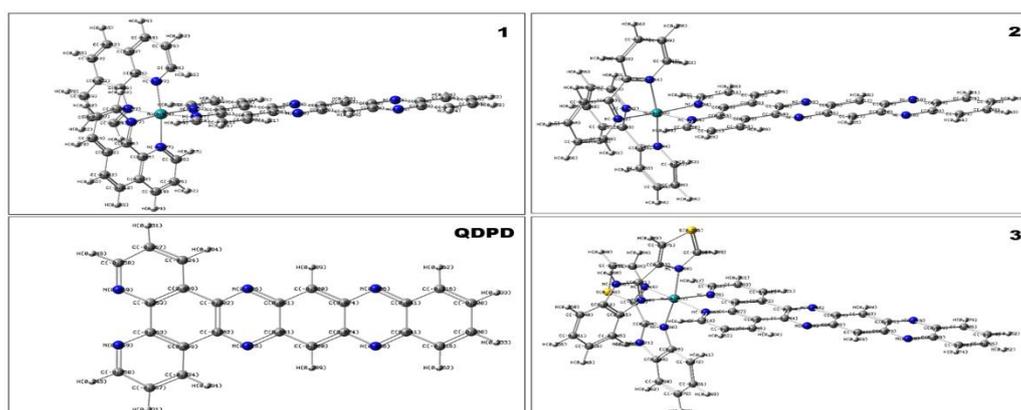
Figure 6. Mulliken charge distribution per atom in QDPD ligand and its Ru Complexes. Qpd.-Ligand, 1. [Ru(phen)$_2$qpd]$^{+2}$. 2. [Ru(bpy)$_2$qpd]$^{+2}$ 3. [Ru(tbz)$_2$qpd]$^{+2}$

The charge distribution of [Ru(phen)$_2$qpd]$^{2+}$ complex represented that the carbons attached with electronegative atoms (sulfur and nitrogen) are positively charged; meanwhile, these electronegative atoms withdraw partial charges, making it positive, whereas Cs bonded to Ns are partial negative may be due to the "greater electropositive character of Ru(II) atom".

Table 5. Selective Mulliken atomic charges distribution of qpd and [Ru(A)₂qpd] complex, performed at B3LYP/ LanL2DZ basis set.

qpd	A = phen	*bpy*	tbz
-	Ru - 0.909327	Ru - 1.464861	Ru - 0.952675
-	N6-0.276738	N6 -0.543732	N6 -0.330042
-	N5-0.276747	N5 -0.543723	N5 -0.249082
-	N4-0.277444	N4 -0.542302	N4 -0.339893
-	N3 -0.277174	N3 -0.542287	N3 -0.267614
N1 -0.132442	N1 -0.277192	N1 -0.534033	N1-0.287698
N2 -0.132365	N2 -0.277441	N2 -0.534057	N2-0.278142
C3 -0.028050	C7 -0.091266	C7 -0.542287	C7-0.287698
C4 0.015953	C8 -0.091252	C8 0.333343	C8 0.039050
C5 0.018551	C9 0.565278	C9 0.331168	C9 0.078288
C6 -0.041547	C10-0.237886	C10 -0.019137	C10-0.021071
N15 -0.129716	N21 0.019212	N48 -0.118361	N28 0.019342
N16 -0.128998	N23 0.019213	N50 -0.118362	N31 0.019092
N23 -0.148471	C12 0.565270	C31 0.128334	C12 0.572499
N26 -0.147460	C54 0.472430	C34 0.128324	C17 0.576634
	N13 0.047818	N40 -0.102475	N20 0.048248
	N16 0.047819	N43 -0.102472	N21 0.048359
			S47 0.368538
			S58 0.396324

The extraordinary negative charge on N(1), N(2), N(3), N(4), N(5), and N(6) atoms are due to their electron withdrawing nature. The N1 and N2 electron withdrawing is more as indicated by highly negative charge as shown in Table 5 and Table S1. Table 6 represents the dipole moment and hyperpolarizability. The total molecular dipole moment of qpd is 4.4954D which is ninety times bigger than the μ of quinoxaline = 0.51 D. The hyper polarizability is 3.2544×10^{-30} esu for qpd ligand and for a Ru - phen complex - 2.75942×10^{-30} esu, whereas for Ru – bpy and Ru - tbz complex the polarizabilities are lower 2.4519×10^{-30} esu and 2.0977×10^{-30} esu respectively.

The development of nonlinear optical materials with better response is significant. Theoretical understanding of factors that influence properties is vital to developing materials with improved optical properties [65].

Table 6. Calculated dipole moment (μₜₒₜ), polarizability (|αₒ|), first hyperpolarizability (βₒ) using B3LYP/LanL2DZ.

Parameter		qpd	Complex1	Complex2	Complex3	
Dipole moment (Debye)	μ_x	4.4949	15.3308	20.2956	-14.2755	
	μ_y	0.0083	0.0004	0.0006	-1.8257	
	μ_z	0.0677	-0.0001	0.0003	1.0613	
	μ_{tot}	4.4954	15.3308	20.2956	14.4308	
Polarizability	A_{xx}	-158.3759	-15.3184	-23.1516	-31.2527	
	A_{yy}	-153.6999	-234.7872	-233.7433	-255.3274	
	A_{zz}	-180.0563	-274.7861	-263.0043	-280.1854	
	A_{xy}	0.1732	-0.0030	0.0009	13.8840	
	A_{xz}	-0.1116	0.0020	0.0000	-2.6505	
	A_{yz}	0.4582	-4.9744	5.4546	7.6791	
	α_o	164.0440	-174.9639	-173.2997	-188.9218	

Hyperpolarizibility	Bxxx	496.7972	-1119.2753	-505.9919	1138.9431
	Byyy	0.4870	0.0425	0.0058	38.4103
	Bzzz	-0.0829	0.0021	0.0231	66.5923
	Bxyy	-113.3825	542.0735	493.0239	-474.0130
	Bxxy	-0.5511	-0.0478	-0.0013	-76.3589
	Bxxz	2.3276	-0.0045	0.0398	-108.2040
	Bxzz	-9.9759	257.8134	296.7082	-302.8252
	Byzz	0.0328	-0.0032	0.0359	-18.1080
	Byyz	0.8900	-0.0034	-0.0296	-21.6206
	Bxyz	-4.3660	-36.1428	43.2940	-67.1107
	β_o	3.2544	- 2.75942	2.451953	2.0977

The influence of the Ru(II) complex binding with DNA was investigated by docking studies using the Patch Dock server. The distinct binding tendencies of the Ru complexes are traced to the distinction in the auxiliary ligand and intercalator length. An interactive mode of binding is observed via docking studies and agrees with the earlier experimental observations. The metal-to-intercalator lengths of complexes are 15.8812, 15.8206, and 15.8691 Å, respectively. It is noteworthy to observe that the shorter length of the Metal - intercalator, which in turn may enhance the stability of the conformer as well as the DNA binding affinity.

Table 7. Binding interactions of the docked poses.

S.No.	Metal Complexes	Patch dock score	Area	ACE (kcal/mol)	Bonding Interactions	Distance (Å)
1	Complex 1	5506	701.90	-669.31	UNK13:N - B:DG19:O4' UNK23:N - A:DC9:O2 A:DC9:C1' - UNK23:N UNK86:H - A:DG7:O3'	3.14135 3.26771 3.49806 2.42995
2	Complex 2	5556	709.10	-652.71	UNK40:N - A:DC9:O2 UNK50:N - B:DG19:O4' A:DC9:C1' - UNK40:N UNK75:H - A:DG10:N3	3.08644 2.34605 3.47158 2.94797
3	Complex 3	5942	761.90	-650.94	UNK21:N - B:DC21:O4' UNK31:N - B:DT20:O4'	3.27401 2.41337

As observed in Table 7, the desolvation energy of the phen complex is more incredible, and the experimental data, Intrinsic binding constants, and desolvation energies for the complexes are in the order 1 > 2 > 3. A careful study of the interactions the DNA poses with complexes reveals that all complexes strongly prefer guanine and cytosine, whereas complex 3 also binds with thymine.

Investigating the absorption, distribution, metabolism, excretion, and toxicity of the so-called ADMET properties of a compound is a crucial step in the drug development process. Usually, toxicities are investigated in animal experiments, which are time-consuming and take animal lives. In silico toxicity, predictions were carried out for the studied complexes. A fast and inexpensive alternative to animal experiments via ProTox-II is a virtual toxicity lab via a web server for in silico toxicity prediction. ProTox-II predicts multiple toxicological endpoints related to a chemical structure [66]. Table S2 of supplementary data shows this virtual toxicity server data indicating that complex 1 with LD50 belongs to class V and complex 2 and 3 class IV, suggesting toxicity.

4. Conclusions

The Ru(II) Polypyridyl complexes are characterized, and their interaction with DNA is studied, indicating that planarity of novel intercalator ligand plays a crucial role in DNA binding. Complex 1 (K_b = 8.0 x 10^5 M^{-1}) binds to DNA more effectively than complexes 2 and 3 (since complex 1 has Phen as an ancillary ligand). The binding affinity is described in order 1 > 2 > 3. The viscosity data indicate that the Ru(II) complexes bind to the DNA via interactive mode. The results recommend that the tenacity of an ancillary ligand ensues their distinctiveness for DNA binding. The quencher effectively quenched the complexes in the absence of DNA.

All complexes show an intense MLCT band due to n →π * transition from HOMO to LUMO molecular orbital energy. The HOMO and LUMO gap for a phen complex is 2.0865 eV compared to the Intercalator (2.5327eV), indicating kinetic stability and its nucleophilic level of sensitivity. Among the three complexes, the phen complex has the longest Intercalator length 15.8812 Å, and also the best optical properties (α = -188.9218 × 10^{-24}esu and β = -

2.75942 $\times$ 10^{-30}esu) provide comprehension of the NLO properties of Ru (II) complexes.

Further molecular docking investigations predicted an octahedral geometry and a DNA binding preference for guanine. The docking investigations also confirm the binding constant information obtained using the absorption and emission techniques. The possibility of emerging the Ru(II) - qpd complexes as a strong DNA probe and NLO material, thereby providing insight into the MLCT shifts and binding affinity upon intercalation of the complex into DNA.

Conflict of interest

The corresponding author states no conflict of interest exists.

Availability of data and material/data availability

All data generated or analyzed during this study are included in this published article [and its supplementary information files].

References

1. M.J. Clark, Ruthenium metallopharmaceuticals, Coordination Chemistry Reviews, **2003**, 236, 209-33.
2. R.W. Sun, D.L. Ma, E.L. Wong, C.M. Che, Some uses of transition metal complexes as anticancer and anti-HIV agents, Dalton Transactions, **2007**, 43, 4884-4892.
3. M. Poursharifi, M.T. Wlodarczyk, A.J. Mieszawska, Nano-based systems and biomacromolecules as carriers for metallodrugs in anticancer therapy, Inorganics, **2018**, 7, 1-19.
4. B.K. Keppler, Metal Complexes in Cancer Chemotherapy, Weinheim, Germany: VCH, **1993**,187-202.
5. E. Thomas, K. Franz, M. Stefan, D. Dimić, I. Morgan, M. Saoud, D. Milenković, Z. Marković,T. Rüffer, J.D. Marković, N. Kaluđerović, Synthesis, Crystallographic Structure, Theoretical Analysis, Molecular Docking Studies, and Biological Activity Evaluation of Binuclear Ru(II)-1-Naphthylhydrazine Complex, Int. J. Mol. Sci., **2023**, 24, 689.
6. N.G. García-Peña, A.M. Caminade, A. Ouali, R. Redón, C.O. Turrin, Solventless synthesis of Ru (0) composites stabilized with polyphosphorhydrazone (PPH) Dendron's and their use in catalysis, RSC advances, **2016**, 6, 64557-64567.
7. R. Hudson, V. Chazelle,M.Bateman, R. Roy, C.J. Li, A. Moores, Sustainable synthesis of magnetic ruthenium-coated iron nanoparticles and application in the catalytic transfer hydrogenation of ketones, ACS Sustainable Chemistry & Engineering, **2015**, 4, 814-820.
8. S. Santoro, V. Sebastian, A.J. Moro, C.A. Portugal, J.C. Lima, I.M. Coelhoso, Development of fluorescent thermoresponsive nanoparticles for temperature monitoring on membrane surfaces, Journal of Colloid and Interface Science, **2017**, 15, 144-1452.
9. R.A. Krause, Synthesis of ruthenium (II) complexes of aromatic chelating heterocycles: Towards the design of luminescent compounds, Coordination Compounds: Synthesis and Medical Application, **2005**, 67, 1-52.
10. D.R. Casimiro, J.H. Richards, J.R. Winkler, H.B. Gray, Electron transfer in ruthenium-modified cytochromes c sigma.-tunneling pathways through aromatic residues, The Journal of Physical Chemistry, **1993**, 97, 13073-13077.
11. D.P. Rillema, G. Allen, T.J. Meyer, D. Conrad, Redox properties of ruthenium (II) tris chelate complexes containing the ligands 2, 2'-bipyrazine, 2, 2'-bipyridine, and 2, 2'-bipyrimidine, Inorganic Chemistry, **1983**, 22, 1617-1622.
12. C.K. Prier, D.A. Rankic, D.W. MacMillan, Visible light photoredox catalysis with transition metal complexes: applications in organic synthesis, Chemical Reviews, **2013**, 10, 5322-5363.
13. E. Tfouni, Photochemical reactions of amminerruthenium (II) complexes, Coordination Chemistry Reviews, **2000**, 1, 281- 305.
14. S. Wolfgang, T.C. Strekas, H.D. Gafney, R.A. Krause, K. Krause, Spectral and photophysical properties of ruthenium (II) 2-(phenylazo) pyridine complexes, Inorganic Chemistry, **1984**, 23, 2650-2655.
15. F. Millett, B. Durham, Design of photoactive ruthenium complexes to study interprotein electron transfer, Biochemistry. **2002**,41, 11315-11324.
16. Y. Qin, Q. Peng, Ruthenium sensitizers and their applications in dye-sensitized solar cells, International Journal of Photoenergy, **2012**, 2012, 1-21.
17. M.K. Nazeeruddin, F. De Angelis, S. Fantacci, A. Selloni, G. Viscardi, P. Liska, Combined experimental and DFT-TDDFT computational study of photoelectrochemical cell ruthenium sensitizers, Journal of the American Chemical Society, **2005**, 127,16835-16847.
18. L. Zeng, Y. Chen, H. Huang, J. Wang, Cyclometalated Ruthenium (II) Anthraquinone complexes exhibit strong anticancer activity in hypoxic tumor cells, Chemistry, **2015**, 21, 15308–15319.
19. F.E. Poynton, S.A. Bright, S. Blasco, D.C. Williams, The development of Ruthenium (II) Polypyridyl complexes and conjugates for invitro cellular and invivo applications, Che.Soc. Rev., **2017**, 4, 7706–7756.
20. A. Juris, V. Balzani, F. Barigelletti, S. Campagna, P. Belser, A. von Zelewsky, Ru(II) Polypyridine Complexes: Photophysics, Photochemistry, Electrochemistry, and

Chemiluminescence, Coordination Chemistry Reviews, **1988**, 84, 285-277.

21. F. Diederich, M. Gómez-López, Supramolecular fullerene chemistry, Chem. Soc. ReV., **1999**, 28, 263-277.

22. M.D. Meijer, G.P.M. van Klink, G. van Koten, Metal-chelating capacities attached to fullerenes, Coordination Chemistry Reviews, **2022**, 230, 141–163.

23. F. D'Souza, O. Ito, H. R. Nalwa, Handbook Org. Elec. Phot, American Scientific Publishers, **2008**, 1, 485-521.

24. R. Chitta, F. D'Souza, Self-assembled tetrapyrrole–fullerene and tetrapyrrole– carbon nanotube donor–acceptor hybrids for light induced electron transfer applications, J. Mater. Chem., **2008**, 18, 1440-1447.

25. D.M. Guldi, T. Da Ros, P. Braiuca, M. Prato, E. Alessio,C60 in the box. A supramolecular C60–porphyrin assembly, J. Mater. Chem., **2002**, 12, 2001-2008.

26. A.F. Collings, C. Critchley, Artificial Photosynthesis: From Basic Biology to Industrial Application; Wiley-VCH Verlag GmbH & Co. KGaA: Weinheim, Germany, **2005**.

27. V. Balzani, M. Clemente-Leo´n, A. Credi, B. Ferrer, M. Venturi, A.H. Flood, J.F. Stoddart, Autonomous artificial nanomotor powered by sunlight Proc, Natl. Acad. Sci., **2006**, 103, 1178-1183.

28. M. Yamada, Y. Tanaka, Y. Yoshimoto, S. Kuroda, I. Shimao, Synthesis and Properties of Diamino-Substituted Dipyrido [3,2-*a*: 2′,3′-*c*]phenazine, Bull. Chem. Soc. Jpn., **1992**, 65, 1006.

29. B.P. Sullivan, D.J. Salmon, T. Meyer, Mixed phosphine 2,2'-bipyridine complexes of ruthenium, Inorg. Chem., **1987**, 17, 3334.

30. N. Navaneetha, K. Aruna, V. Ravi Kumar, A. Praveen Kumar, S. Satyanarayana, A Biophysical Study of Ru(II) Polypyridyl Complex, Properties and its Interaction with DNA, Journal of Fluorescence, **2022**, 32, 1211-1228.

31. N. Navaneetha, K. Aruna, V. Ravi Kumar, A. Praveen Kumar, S. Satyanarayana, Binding and Photocleavage studies of Ru (II) Polypyridyl Complexes with DNA: An In Silico and Antibacterial activity, Analytical Chemistry Letters, **2022**, 12, 266–282.

32. L.H. Han, C.R. Zhang, J.W. Zhe, N.Z. Jin, Y.L. Shen, W. Wang, J.J. Gong, Y.H. Chen, Z.J. Liu, Understanding the electronic structures and absorption properties of porphyrin sensitizers YD2 and YD2-o-C8 for dye-sensitized solar cells, Int. J. Mol. Sci., **2013**, 14, 20171-20188.

33. T. Mihaylov, N. Trendafilova, I. Kostova, I. Georgieva, G. Bauer, DFT modeling and spectroscopic study of metal-ligand bonding in La(III) complex of coumarin-3-carboxylic acid, Chem. Phys., **2006**, 327, 209-219.

34. M.J. Frisch, G.W. Trucks, H.B. Schlegel, G.E. Scuseria, M.A. Robb, J.R. Cheeseman, G. Scalmani, V. Barone, B. Mennucci, G.A. Petersson, Gaussian 09, Revision D. 01, Gaussian Inc, Wallingford, **2009**.

35. R.E. Stratmann, G.E. Scuseria, M.J. Frisch, An efficient implementation of time-dependent density-functional theory for the calculation of excitation energies of large molecules, J. Chem. Phys., **1998**, 109, 8218–8224.

36. R.G. Parr, Density Functional Theory, Annual Review of Physical Chemistry, **1983**, 34, 631-656.

37. C. Lee, W. Yang, R.G. Parr, Development of the Colle-Salvetti correlation-energy formula into a functional of the electron density, Physical Review B, **1988**, 37, 785-789.

38. A.B. Punnarao, K. Gulati, N. Joshi, D.K. Deb, D. Rambabu, W. Kaminsky, K.M. Poluri, M.R. Kollipara, Molecular structure, spectroscopic investigation and quantum chemical calculations of Ruthenium (II) complex of isoniazid ligand, Inorg Chim Acta, **2017**, 1693, 30488.

39. N.A. Ogorodnikova, On invariance of the Mulliken substituent-induced charge changes in quantum-chemical calculations of different levels, J. Mol. Struct., **2009**, 894, 41–49.

40. A.N. El-Ghamaz, M.A. Diab, A.A. El-Bindary, Geometrical structure and optical properties of antipyrine Schiff base derivatives, Mater Sci Semicond Process, **2014**, 27, 521–531.

41. A.Z. El-Sonbati, M.A. Diab, A.A. El-Bindary, S.M. Morgan, Supramolecular spectroscopic and thermal studies of azodye complexes, Spectrochim Acta Part A Mol Biomol Spectrosc, **2014**, 127, 310–328.

42. A.Z. El-Sonbati, M.A. Diab, A.A. El-Bindary, Molecular docking, DNA binding, thermal studies and antimicrobial activities of Schiff base complexes. J. Mol. Liq., **2016**, 218, 434–456.

43. V.M. Geskin, C, Lambert, J.L. Bredas, Origin of High Second- and Third-Order Nonlinear Optical Response in Ammonio/Borato Diphenylpolyene Zwitterions: the Remarkable Role of Polarized Aromatic Groups, J Am Chem Soc., **2003**, 125, 15651.

44. V. Barone, M. Cossi, J. Thomasi, Geometry optimization of molecular structures in solution by the polarizable continuum model, J ComputChem., **1998**, 19, 404-417.

45. N.A. Ogorodnikova, On invariance of the Mulliken substituent-induced charge changes in quantum-chemical calculations of different levels, J. Mol. Struct., **2009**, 894, 41–49.

46. D. Schneidman-Duhovny, Y. Inbar, R. Nussinov, H.J. Wolfson, PatchDock and SymmDock: servers for rigid and symmetric docking, Nucleic Acids Res., **2005**, 33, W363–W367.

47. T.P. James, M. Matshwele , O. Sebusi,
    D. Mapolelo, M. Leteane, G. Lebogang, D.
    Julius, O. Nkwe, and F. Nareetsile, Antibacterial
    Activity of 2-Picolyl-polypyridyl-Based
    Ruthenium (II/III) Complexes on Non-Drug-
    Resistant and Drug-Resistant Bacteria,
    Bioinorganic Chemistry and Applications, **2021**,
    2021, 5563209.

48. A.D. Allen, C.V. Senoff, Preparation and infrared
    spectra of some ammine complexes of
    ruthenium(II) and ruthenium(III), Can. J. Chem.,
    1967, 45, 1337-1341.

49. P.V. Reddy, M.R. Reddy, S. Satyanarayana,
    Design, Synthesis, DNA binding affinity,
    cytotoxicity, apoptosis and cell cycle arrest of
    Ru(II) polypyridyl complexes, Anal
    Biochem., **2015**, 15, 49-58.

50. R.K. Gupta, R. Pandey, G. Sharma, DNA
    Binding and AntiCancer Activity of Redox-
    Active Heteroleptic Piano-Stool Ru(II), Rh(III),
    and Ir(III) Complexes Containing 4-(2-
    Methoxypyridyl) phenyldipyrromethene, Inorg
    Chem, **2013**, 52, 3687–3698.

51. A.E. Friedman, J.C. Chambron, J.P. Sauvage,
    N.J. Turro and J.K. Barton, A molecular light
    switch for DNA: $Ru(bpy)_2(dppz)^{2+}$, J. Am. Chem.
    Soc., **1990**, 112, 4960-4962.

52. J.B. Lepecq, C. Paoletti, A fluorescent complex
    between ethidium bromide and nucleic acids. J
    Mol Biol., **1967**, 27, 87–106.

53. R.K. Vuradi, S. Avudoddi, V.R. Putta, Synthesis,
    Characterization and Luminescence Sensitivity
    with Variance in pH, DNA and BSA Binding
    Studies of Ru(II) Polypyridyl Complexes, J
    Fluoresc, **2017**, 27, 939–952.

54. J.B. Chaires, Energetics of drug–DNA
    interactions, Biopolymers, **1997**, 44, 201–215.

55. S. Satyanarayana, J.C. Dabrowiak, J.B. Chaires,
    Tris(phenanthroline)ruthenium(II) enantiomer
    interactions with DNA: Mode and specificity of
    binding, Biochemistry, **1993**, 32, 2573–2584.

56. R.K. Vuradi, V.R. Putta, D. Nancherla, S.
    Sirasani, Luminescent Behavior of Ru(II)
    Polypyridyl Morpholine Complexes, Synthesis,
    Characterization, DNA, Protein Binding, Sensor

57. Effect of Ions/Solvents and Docking Studies, J
    Fluoresc., **2016**, 26, 689–701.

57. M. Ahmadnezhad, M. Darvish Ganji, M.
    Rezvani, Theoretical studies on the geometrical
    and electronic structures of supramolecule
    bis(2,2′bipyridine)-5-amino-1,10-phenanthroline
    ruthenium(II)/functionalized SWCNT dyads, J
    Physics and Chemistry of Solids, **2015**, 86,
    148-154.

58. R.G. Parr, L. Szentpály, S. Liu, Electrophilicity
    Index, J Am Chem Soc., **1999**, 121, 1922.

59. N. Choudhary, S. Bee, A. Gupta, P. Tandon,
    Comparative vibrational spectroscopic studies,
    HOMO–LUMO and NBO analysis of *N*-
    (phenyl)-2,2-dichloroacetamide, *N*-(2-chloro
    phenyl)-2,2-dichloroacetamide and *N*-(4-chloro
    phenyl)-2,2-dichloroacetamide based on density
    functional theory, Comp Theor Chem., **2013**,
    1016, 8-21.

60. K. Fukui, Role of frontier orbitals in chemical
    reactions, Science, **1982**, 218, 747.

61. G. Gece, The Use of Quantum Chemical
    Methods in Corrosion Inhibitor Studies, Corros
    Sci., **2008**, 50, 2981-2992.

62. L. Sinha, O. Prasad, V. Narayan, S.R. Shukla,
    Raman, FT-IR spectroscopic analysis and first-
    order hyperpolarizability of 3-benzoyl-5-
    chlorouracil by first principles, J Mol Simul.,
    2011, 37, 153-163.

63. M. Govindarajan, M. Karabacak, Spectroscopic
    properties, NLO, HOMO-LUMO and NBO
    analysis of 2,5-Lutidine, Spectrochim Acta A,
    2012, 96, 421.

64. S. Guidara, A.B. Ahmed, Y. Abid, H. Feki,
    Molecular structure, vibrational spectra and
    nonlinear optical properties of 2,5-
    dimethylanilinium chloride monohydrate: a
    density functional theory approach, Spectrochim
    Acta A, **2014**, 127, 275-285.

65. D. F. Eaton, Nonlinear optical materials, Science,
    1991, 253, 281-289.

66. M.N. Drwal, P. Banerjee, M. Dunkel, M.R.
    Wettig, R. Preissner, ProTox: a web server for
    the in silico prediction of rodent oral toxicity,
    Nucleic Acids Res., **2014**, 42, W53-W58.

The following substances were purchased from Merck: 1, 10-phenanthroline monohydrate (phen), 2, 2'-bipyridine (bpy), 2-(1H-Pyrrol-2-yl)-1H-indole (tbz) CT-DNA (Calf thymus DNA) was bought from Aldrich, and stored at 20°C. All studies used 18.2 mX ultrapure Milli-Q water. All additional chemicals and solvents came from already-established local sources. Before usage, all solvents underwent normal processes for purification [1]. A stock solution of metal complexes was created by dissolving calculated amounts of metal complexes in DMSO and adjusting the concentrations with the right buffer.

A PerkinElmer 1605 Fourier transform I.R. spectrometer was utilized to record the I.R. spectra on KBr discs. Dimethyl-d_6 sulfoxide (DMSO-d_6) was used as the solvent, and tetramethyl silane served as the internal standard to record the ^{1}H NMR spectra on a Bruker 400-MHz spectrometer at room temperature. The UV-VISIBLE spectra were captured with a Shimadzu UV-2600 spectrophotometer. The luminescence spectrum data were recorded using a Spectrofluorometer (serial number of the Cary Eclipse instrument, MY12400004) to assess the binding constant.

Electronic absorption studies

DNA binding studies were conducted to study DNA-binding interactions. Double distilled water was used to prepare each solution. In Tris buffer (5mM Tris-HCL, 50 mM NaCl, pH 7.1), investigations involving the interaction of Ru(II) complex with CT-DNA were carried out. After preparation, the stock solution of CT-DNA was kept at 4° C in the dark and used within three days. Ru (II) complex stock solutions in DMSO were prepared. By treating a fixed concentration of complex (10μM) with increments (0-120μM) of the protein-free DNA stock solution (0.617×10^{-4} M) [2], the absorption experiment for steps 1-3 in the buffer was carried out. Solutions were given 5 min to incubate before recording the complex-DNA mixture's absorption spectra. After each measurement, UV-vis spectra were taken. After each addition of DNA solution, the intrinsic binding constant (K_b) is calculated by using Equation (1) [3].

$$[DNA]/(\varepsilon_a - \varepsilon_f) = [DNA]/(\varepsilon_b - \varepsilon_f) + 1/K_b(\varepsilon_b - \varepsilon_f) \qquad (1)$$

ε_a, ε_b, and ε_f represent the apparent absorption coefficient $A_{obs}/[complex]$, the extinction coefficient for the complex in its fully bound form, and the extinction coefficient for the free complex, respectively. [DNA] is the concentration of DNA. The intrinsic binding constant is represented K_b, a graph plotted between $[DNA] / (\varepsilon_a - \varepsilon_f)$ and [DNA]. K_b is derived using the slope-to-intercept ratio.

Fluorescence Emission

They increased the DNA concentration until the complex concentration was fixed and made measurements of the Ru(II) complexes' emission intensities. The spectra were acquired between 540nm and 760nm. Equation 2 was used to calculate the binding constant [4].

$$C_b = C_t[(F - F_0)/(F_{max} - F_0)] \qquad (2)$$

Where F_0 is the intensity in the absence of DNA, F is the observed fluorescence emission intensity at a specific DNA concentration, and F_{max} is the intensity of the maximum complex bound to DNA. C_t stands for the total complex concentration.

$$r/C_f = K_b(1 - nr) \qquad (3)$$

SUPPLEMENTARY DATA

A graph between r/C_f versus r was used to derive the binding constant using the Scatchard equation 3, where r is the C_b/[DNA] ratio and C_f is the concentration of the free complex. The excitation wavelength for the fluorescence titration investigations was fixed at 425 nm, and the spectra were acquired by altering the pH of the solutions.

Quenching studies

This luminescent experiment expanded quenching investigations with [Fe(CN)6]-4 to better understand how these complexes bind to DNA. Fluorescence quenching studies with $[Fe(CN)_6]^{-4}$ provide additional insight into the complexes binding to DNA. To the 3mL of the complex, the quencher (0.01M) is added in Tris HCl buffer in the presence of DNA, and the absence of DNA (1:20 and 1:200, i.e., in excess) was used to execute emission quenching investigations at room temperature. Sterne Volmer equation 4 was applied to determine the quenching constant K_{sv}. Where Q is the concentration of the quencher, I_0 and I are the fluorescence intensities in the presence and absence of the quencher, respectively, and K_{sv} is a linear Sterne Volmer quenching constant that may be calculated from the slope [5]

$$I_0/I = 1 + K_{SV}[Q] \tag{4}$$

Viscosity studies

Viscosity investigations were done by using an Ostwald viscometer, which was submerged in a thermostat bath in order to maintain a consistent temperature of 30 ± 0.1^0C using BPE buffer (6 mM Na_2HPO_4, 2 mM NaH_2PO_4, 1Mm Na_2EDTA, pH=7.0). To reduce the complexes brought on by DNA flexibility, the 200 base pair average length CT-DNA samples were processed by sonication [6]. An average flow time was computed after each sample was repeated three times, and the flow time was recorded using a digital stopwatch. The estimated information was displayed as $(\eta/\eta_0)^{1/3}$ vs [Ru(II)/[DNA] concentration [7], where η is the viscosity of DNA in the presence of the complex and η_0 is the viscosity of DNA alone. Viscosity values can be calculated from the observed 't' using DNA-containing solutions' flow time corrected for the buffer's flow time alone (t_0)[8, 9].

References

1. D. Perrin, W.L.F. Annarego, D.R. Perrin. Purification of Laboratory Chemicals, 2nd Edn, Pergamon Press, New York, NY (1980).

2. E.A. Steck, A.R. Day. J. Am. Chem. Soc., 65, 452 (1943). https://doi.org/10.1021/ja01243a043

3. A. Wolfe, G.H. Shimer, T. Meehan. Biochem., 26, 6392 (1987). https://doi.org/10.1021/bi00394a013

4. J.D. McGhee, P.H. von Hippel. J. Mol. Biol., 86, 469 (1974). https://doi.org/10.1016/0022-2836(74)90031-X

5. Lakowicz, J. R.; Weber, G. Quenching of Fluorescence by Oxygen. A Probe for Structural Fluctuations in Macromolecules. Biochemistry. 1973, 12, 4161–4170. https://doi.org/10.1021/bi00745a020

6. J.B. Chaires, N. Dattagupta, D.M. Crothers. Biochem., 21, 3927 (1982). 1982 https://doi.org/10.1021/bi00260a004

7. S. Satyanarayana, J.C. Dabrowiak, J.B. Chaires. Biochem., 32, 2573 (1993).

8. Satyanarayana S, Dabrowiak JC, Chaires JB (1992) Neither. DELTA.- nor.LAMBDA.- tris(phenanthroline)ruthenium(II) binds to DNA by classical intercalation. Biochemistry 31:9319–9324. https:// doi. org/ 10. 1021/ bi001 54a001

9. Long EC, Barton JK (1990) On demonstrating DNA intercalation. Acc Chem Res 23(9):271–273. https:// doi. org/ 10. 1021/ ar00177a001
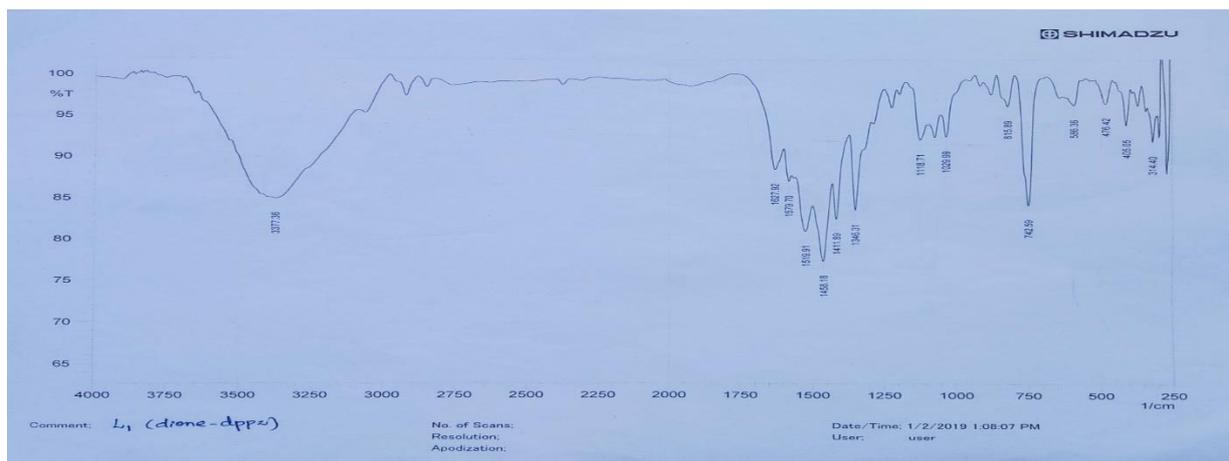
Figure S1. IR Spectra of Intercalator, Ligand qpd.
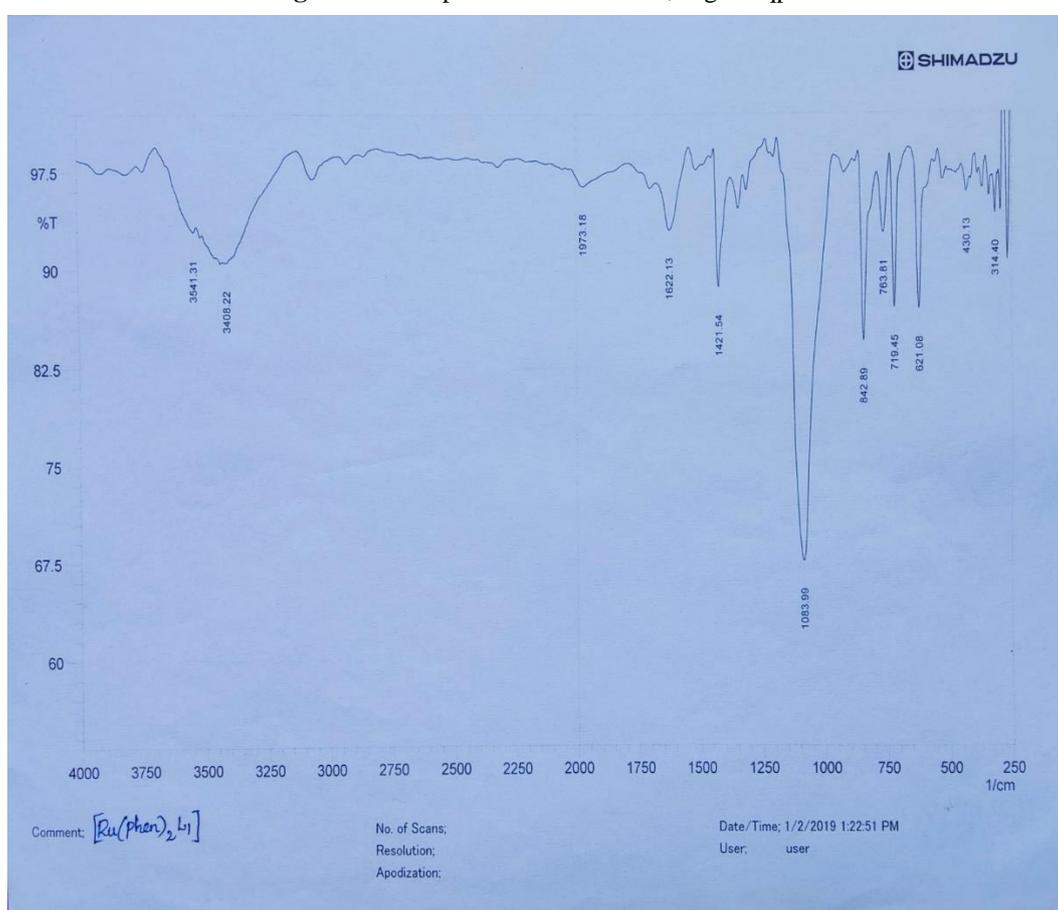
Figure S2. IR Spectra of $[Ru(phen)_2\ qpd\ ]^{2+}$
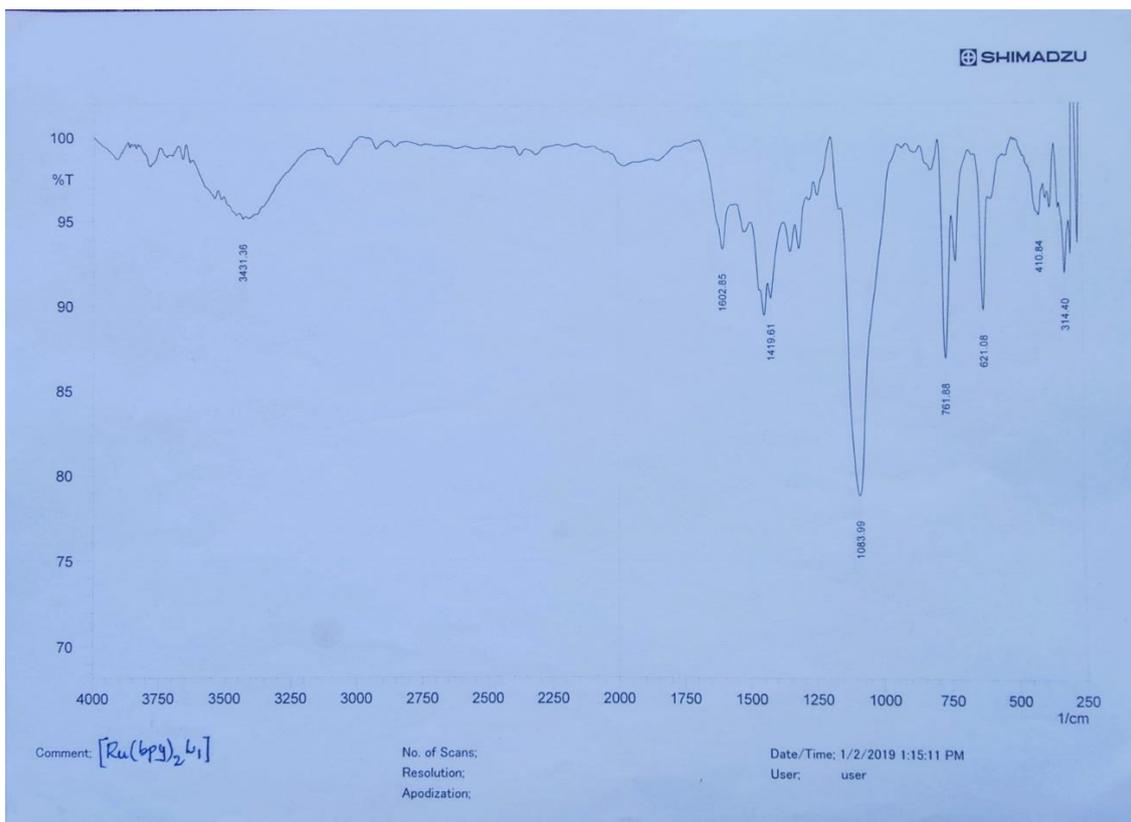
Figure S3. IR Spectra of [Ru(bpy)$_2$ qpd]$^{2+}$
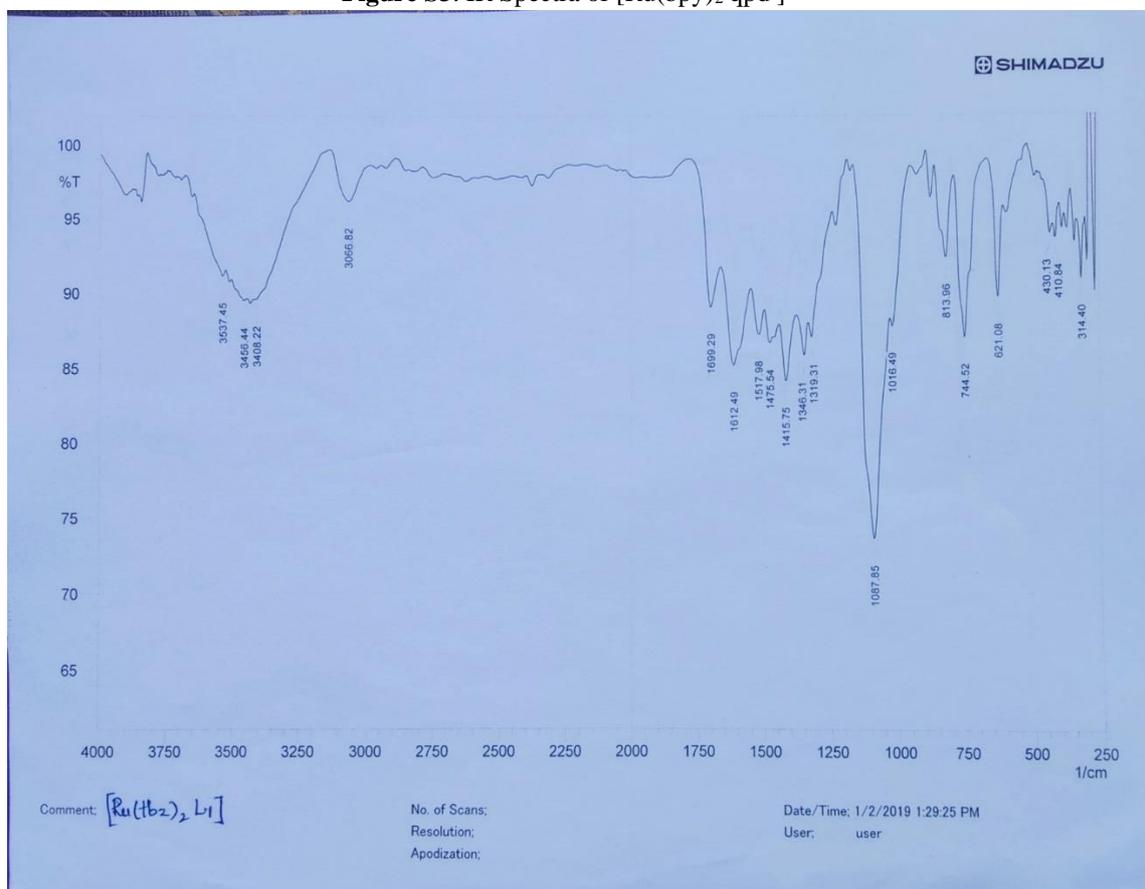
Figure S4. IR Spectra of [Ru(tbz)$_2$ qpd]$^{2+}$
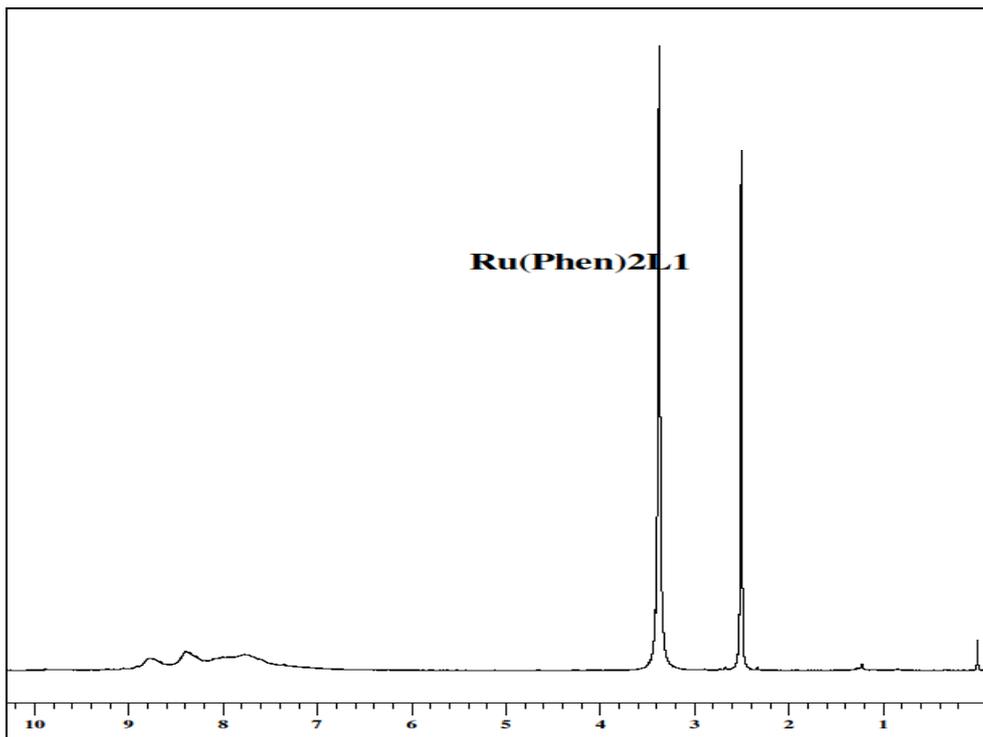
Figure S5. ^{1}H NMR Spectra of [Ru(phen)$_{2}$ qpd]$^{2+}$
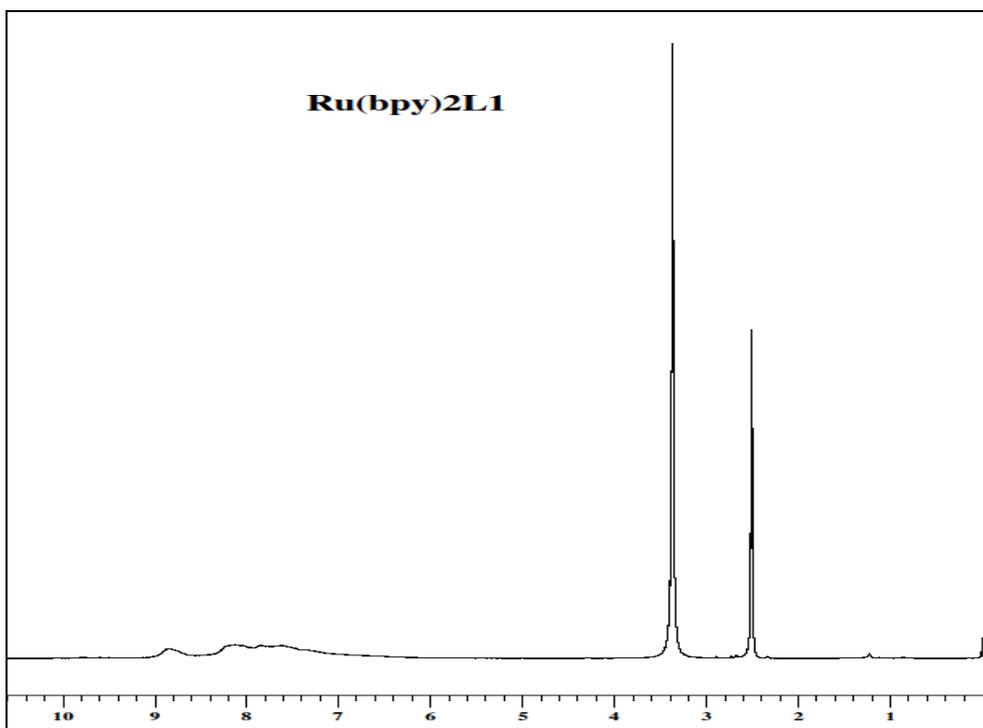
Figure S6. ^{1}H NMR Spectra of [Ru(bpy)$_{2}$ qpd]$^{2+}$
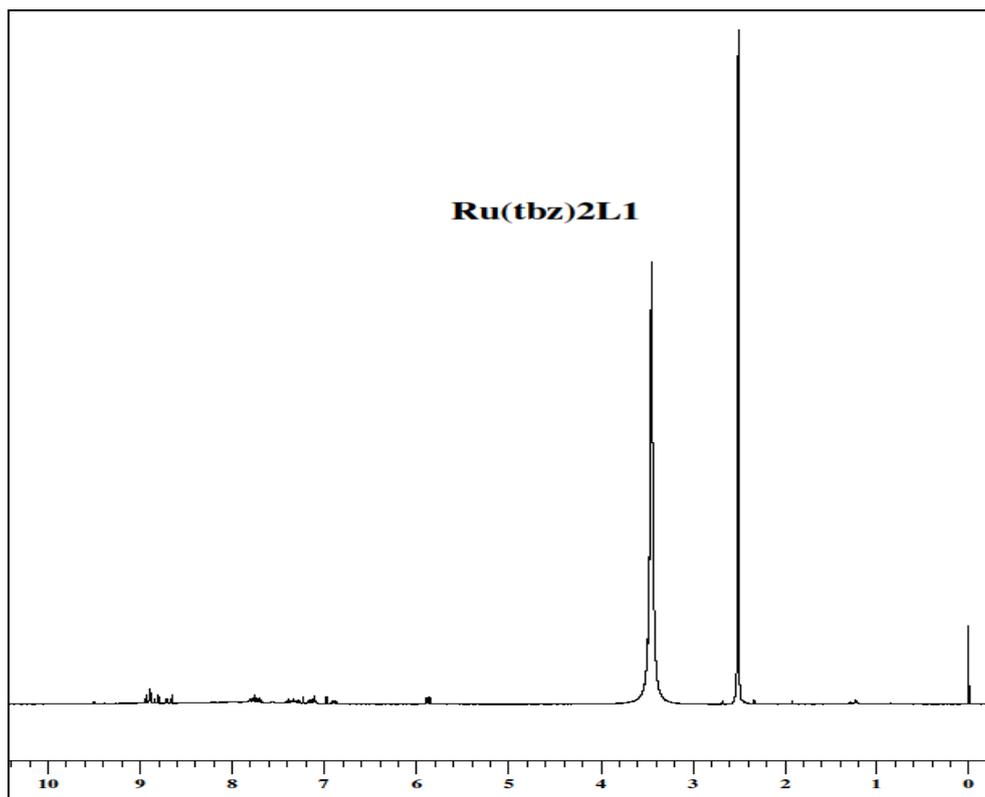
Figure S7. ^{1}H NMR Spectra of [Ru(tbz)$_2$ qpd]$^{2+}$
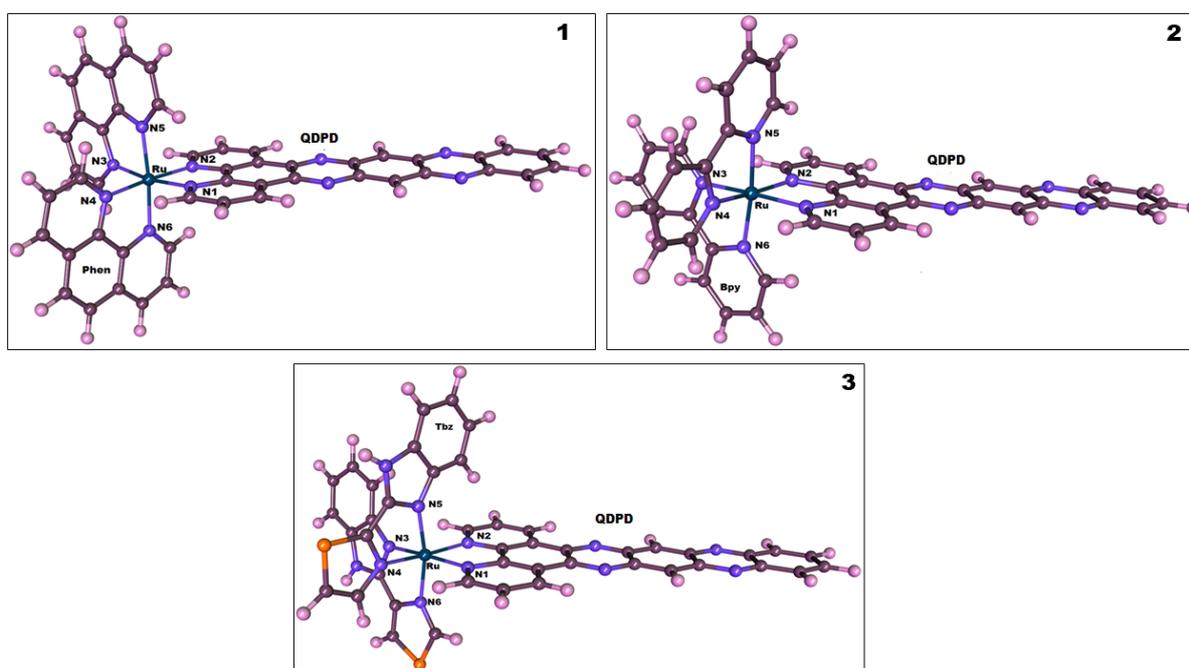
Figure S8. 3D model of the Ru – complexes.

(1) [Ru(phen)$_2$(qpd)]$^{+2}$, (2) [Ru(bpy)$_2$(qpd)]$^{+2}$, (3) [Ru(tbz)$_2$(qpd)]$^{+2}$]

Table S2. Theoretical ADME and predicted LD50.

Property	PHEN	BPY	TBZ
Mol. Wt	851.92	803.88	894.01
Number of hydrogen bond acceptors	39	39	41
Number of hydrogen bond donors	6	6	8
Number of atoms	93	89	91
Number of bonds	108	102	106
Molecular refractivity	260.98	250.61	276.34
Topological Polar Surface Area	194.66	194.66	262.21
octanol/water partition coefficient(logP)	4.12	7.31	8.55
Predicted LD50	5000mg/kg	1000mg/kg	1000mg/kg